

Improved identifiability of cardiac AP model parameters by physiological constraints

1

Gradient-based parameter optimization to determine membrane ionic current composition of human induced pluripotent stem cell-derived cardiomyocytes

Hirohiko Kohjitani¹, Shigeya Koda², Yukiko Himeno², Takeru Makiyama¹, Yuta Yamamoto¹, Daisuke Yoshinaga³, Yimin Wuriyanghai¹, Asami Kashiwa¹, Futoshi Toyoda⁴, Yixin Zhang², Akira Amano², Akinori Noma², Takeshi Kimura¹

¹Department of Cardiovascular Medicine, Kyoto University Graduate School of Medicine, Kyoto, Japan

²Graduate School of Life Sciences, Ritsumeikan University, Kusatsu, Japan

³Department Pediatrics, Kyoto University Graduate School of Medicine, Kyoto, Japan

⁴Department of Physiology, Shiga University of Medical Science, Otsu, Japan

* Correspondence:

Akira Amano

Keywords: Parameter optimization method, hiPSC-CMs, Cardiac action potential, Mathematical model, Computer simulation

Abbreviations

hiPSC-CMs; human induced pluripotent stem cell-derived cardiomyocytes

AP; action potential

MDP; the maximum diastolic potential

SDD; slow diastolic depolarization

Improved identifiability of cardiac AP model parameters by physiological constraints

2

- 27 I_m ; membrane current
- 28 V_m ; membrane voltage
- 29 orp; optimization of randomized model parameters
- 30 PS; pattern search method
- 31 BP; base point for searching minimum MSE in the Pattern Search
- 32 NP; searching point in reference to BP in the Pattern Search
- 33 MSE; mean square error between two different V_m records
- 34 stp; step size to move NP
- 35 x; subscript to represent membrane current such as I_{Na} , I_{CaL} , I_{K1} , I_{ha} , I_{Kr} , I_{Kur} , I_{Ks} and I_{bNSC}
- 36

Improved identifiability of cardiac AP model parameters by physiological constraints

3

1. Abstract

Premature cardiac myocytes derived from human-induced pluripotent stem cells (hiPSC-CMs) show heterogeneous action potentials (APs), most probably because of different expression patterns of membrane ionic currents. We aim to develop a method of determining expression patterns of functional channels in terms of the whole-cell ionic conductances (G_x) using individual spontaneous AP configurations. However, it has been suggested that apparently identical AP configurations were obtained by different sets of ionic currents in a mathematical model of cardiac membrane excitation. If so, the inverse problem of G_x estimation might not be solved. We computationally tested the feasibility of the gradient-based optimization method. For realistic examination, conventional 'cell-specific models' were prepared by superimposing the model output of AP on each experimental AP record by the conventional manual adjustment of G_x s of the baseline model. Then, G_x s of 4 ~ 6 major ionic currents of the 'cell-specific models' were randomized within a range of $\pm 5 \sim 15\%$ and were used as initial parameter sets for the gradient-based automatic G_x s recovery by decreasing the mean square error (MSE) between the target and model output. When plotted all data points of MSE - G_x relation during the optimization, we found that the randomized population of G_x s progressively converged to the original value of the cell-specific model with decreasing MSE. To confirm the absence of any other local minimum in the global search space, we mapped the MSE by randomizing G_x s over a range of 0.1 ~ 10 times the control. No additional local minimum of MSE was obvious in the whole parameter space besides the global minimum of MSE at the default model parameter.

2. Introduction

During more than a half-century, the biophysical characteristics of ion transporting molecules (channels and ion exchangers) have been extensively analyzed, and biophysical models of each functional component have largely been detailed [1–4] (for human-induced pluripotent stem cells (hiPSC-CMs) see [5–7]). In addition, various composite cell models, including the membrane excitation, cell contraction, and the homeostasis of the intracellular ionic composition, have been developed by integrating mathematical models at molecular levels into the cardiac cell models [8–11]. These models have already been quite useful in

Improved identifiability of cardiac AP model parameters by physiological constraints

4

visualizing individual currents underlying the action potential (AP) configuration under various experimental conditions in matured cardiac myocytes. However, the utility of these mathematical cell models has been limited because of the lack of extensive validation for the accuracy of the model output. This is the drawback of the subjective manual fitting used in almost all mathematical cardiac cell models so far published. A new challenge of such mechanistic models of cardiac membrane excitation might be an examination in a very different paradigm to assess if the large but continuous variety of cardiac AP configurations, for example, those recorded in the hiPSC-CMs, can be reconstructed by applying the automatic parameter optimization method to the human cardiac cell models.

The automatic parameter optimization technique has been used to determine parameters objectively in a wide range of various biological models (in cardiac electrophysiology; [12–15], in the systems pharmacology; [16–20]). Because of this utility, a large variety of improvements have been made in the area of information technology [21,22]. However, in electrophysiology, it has been suggested that different combinations of model parameters can produce APs, which are very similar[23–25] (see also [13]). It has been considered that the determination of current density at high fidelity and accuracy requires additional improvements to the optimization method in the cardiac cell model because of complex interactions among ionic currents underlying the membrane excitation (see [26], for review; [23]).

The final goal of our study is to develop an objective and accurate method of determining the current profile (that is, the expression level of functional ionic currents) underlying individual AP configurations. As a case study, we select a large variety of AP configurations in the hiPSC-CMs, which are difficult to classify into the conventional nodal-, atrial- or ventricular-types. Nevertheless, it has been clarified that the molecular bases of the ion channels expressed in the hiPSC-CMs well correspond to those in the adult cardiac myocytes (GSE154580 [GEO Accession viewer \(nih.gov\)](https://www.ncbi.nlm.nih.gov/geo/query/acc.cgi?acc=GSE154580)). Thus, we use the human ventricular cell model (hVC model, [11]) for the baseline model. In the present study, we computationally examine the feasibility of the basic gradient-based optimization method, pattern search (PS) algorithm [21,27,28] in the model of cardiac AP generation. We prepared a given AP configuration using each 'cell specific model', which was prepared by the conventional manual fitting of the hVC model to the respective experimental recordings. To assess the

Improved identifiability of cardiac AP model parameters by physiological constraints

5

accuracy of the PS method of parameter optimization, this AP waveform generated by the cell-specific model was used as a target of the optimization. Then, the initial set of parameters for the optimization was prepared by uniform randomization centered around the model's default values. The PS algorithm should return the original parameters by decreasing the error function (MSE) between the modified model output and target AP waveforms. The accuracy of optimization was definitely judged by recovering of the original values of each ionic current amplitude as the MSE progressively decreased toward zero.

3. Materials and Methods

3.1. The baseline model of hiPSC-CM membrane excitation

The baseline model of hiPSC-CMs was essentially the same as the human ventricular cell model (hVC model), which has been fully described in references [10,11] and shares many comparable characteristics with other human models so far published [8,9]. The model structure of the hVC model consists of the cell membrane with a number of ionic channel species and a few ion transporters, the sarcoplasmic reticulum equipped with the Ca^{2+} pump (SERCA), and the refined Ca^{2+} releasing units coupled with the L-type Ca^{2+} channels on the cell membrane at the nano-scale dyadic space, the contractile fibers, and the cytosolic three Ca^{2+} diffusion spaces containing several Ca^{2+} -binding proteins (Fig S1). All model equations and abbreviations are in Supplemental Materials.

The source code of the present hiPSC-CM model was written in VB.Net and is available from our e-Heart website (<http://www.eheartsim.com/en/downloads/>).

The kinetics of the ionic currents in the baseline model were readjusted according to new experimental measurements if available in the hiPSC-CMs [29] (Fig S2). In the present study, the net membrane current (I_{tot_cell}) is calculated as the sum of nine ion channel currents and two ion transporters (I_{NaK} and I_{NCX}) (Eq 1).

$$I_{tot_cell} = I_{Na} + I_{CaL} + I_{ha} + I_{K1} + I_{Kr} + I_{Ks} + I_{Kur} + I_{Kto} + I_{bNSC} + I_{NaK} + I_{NCX} \quad Eq \ 1$$

Improved identifiability of cardiac AP model parameters by physiological constraints

6

The membrane excitation of the model is generated by charging and discharging the membrane capacitance (C_m) by the net ionic current (I_{tot_cell}) across the cell membrane (Eq 2). The driving force for the ionic current is given by the potential difference between V_m and the equilibrium potential (E_x) (Eq 3). The net electrical conductance of the channel is changed by the dynamic changes in the open probability (pO) of the channel, which is mostly V_m -dependent through the V_m -dependent rate constants (α, β) of the opening and closing conformation changes of the channel (Eqs 4 and 5).

$$\frac{dV_m}{dt} = -\frac{I_{tot_cell}}{C_m} = -\frac{\sum I_x}{C_m} \quad \text{Eq 2}$$

$$I_x = \bar{G}_x \cdot pO \cdot (V_m - E_x) \quad \text{Eq 3}$$

$$\frac{dpO}{dt} = \alpha \cdot (1 - pO) - \beta \cdot pO \quad \text{Eq 4}$$

$$[\alpha \ \beta]^T = f(V_m) \quad \text{Eq 5}$$

The exchange of $3\text{Na}^+ / 2\text{K}^+$ by the Na/K pump and the $3\text{Na}^+ / 1\text{Ca}^{2+}$ exchange by the NCX also generate sizeable fractions of membrane ionic current, I_{NaK} , and I_{NCX} , respectively. We excluded background currents of much smaller amplitude, such as I_{KACH} , I_{KATP} , I_{LCCa} and I_{Cab} , from the parameter optimization and adjusted only the non-selective background cation current (I_{bNSC}) of significant amplitude for the sake of simplicity [30–32]. The I_{bNSC} is re-defined in the present study as a time-independent net current, which remained after blocking all time-dependent currents.

3.2. The computational parameter optimization

The whole cell conductance G_x of a given current system (x) is modified by multiplying the limiting conductance \bar{G}_x (Eq 3) of the baseline model by a scaling factor sf_x (Eq 6) and are used for the parameter optimization.

$$G_x = \bar{G}_x \cdot sf_x \quad \text{Eq 6}$$

The mean square error (MSE) function (Eq 7) was used in the parameter optimization, where $V_{m,a}$ represents adaptive V_m (the model output) generated by adjusting sf_x s of the baseline model. The target $V_{m,t}$ represents the AP of the intact baseline model.

Improved identifiability of cardiac AP model parameters by physiological constraints

7

$$MSE = \frac{\sum (V_{m,a} - V_{m,t})^2}{N} \quad \text{Eq 7}$$

The MSE was stabilized by obtaining a quasi-stable rhythm of spontaneous APs through continuous numerical integration of the model, usually 30 ~ 100 spontaneous cycles were calculated for a new set of sf_x s. The MSE was calculated within a time window. The width of this time window was adjusted according to the AP phase of interest. N is the number of digitized V_m points with a time interval of 0.1 ms.

In the usual parameter optimization, the $V_{m,a}$ is generated by modifying the baseline model for comparison with the experimental record ($V_{m,t} = V_{m,rec}$). However, to evaluate the identifiability of the parameter optimization, a simple approach was taken in the present study. Namely, we used the manually adjusted 'cell-specific' model for the target ($V_{m,t}$), which was nearly identical to $V_{m,rec}$. More importantly, the 'cell-specific' V_m is totally free from extra-fluctuations (noise), which were observed in almost all AP recordings in hiPSC-CMs. In the optimization process, the initial value of each optimization parameter was prepared by randomizing the sf_x s of the cell-specific model by $\pm 5\sim 15\%$ at the beginning of each run of PS ($V_{m,orp}$) in Eq 8 and the PS runs of several hundred were repeated. Thus, the error function is,

$$MSE = \frac{\sum (V_{m,orp} - V_{m,t})^2}{N} \quad \text{Eq 8}$$

We call this optimization method 'orp test' in the present study.

The advantage of using a manually adjusted cell model for the optimization target is that the accuracy of parameter optimization is proved by recovering all $sf_x = 1$ independently from the randomized initial parameter set. Note the same approach was used in [23] in evaluating the accuracy of the parameter optimization by applying the genetic algorithm (GA) to the TNNP model of the human ventricular cell [33].

The optimization of using the randomized initial model parameters were repeated for more than 200 runs. Thus, the orp test might be classified in a 'multi-run optimization'. The distribution of the sf_x data points obtained during all test runs was plotted in a single sf_x -MSE coordinate to examine the convergence of individual sf_x s with the progress of the orp test.

163

Improved identifiability of cardiac AP model parameters by physiological constraints

8

3.3. The pattern search method for the optimization

For a system showing the relatively simple gradient of MSE along the parameter axis, the gradient-based optimization methods are more efficient in general than the stochastic methods for this kind of objective function. We used one of the basic gradient-based optimization methods, the PS algorithm. The computer program code of the pattern search [34] is simple (see Supplemental Materials) and does not require derivatives of the objective function. We implemented the code into a homemade program for data analysis (in VB) to improve the method for better resolution and to save computation time.

The primary PS method uses a base and new points [27]. In brief, sf_x is coded with symbols BP_x and NP_x in the computer program, representing a base point (BP_x) and a new searching point (NP_x), respectively. Namely, MSE is calculated on each movement of NP_x by adding or subtracting a given step size (stp) to the BP_x , and the search direction is decided by the smaller MSE. Then, the whole mathematical model is numerically integrated (Eqs 2, 3, 4, and 5) using NP_x to reconstruct the time course of AP ($V_{m,a}$). This adjustment is conducted sequentially for each of the 4~6 selected currents in a single cycle of optimization. The cycle is repeated until no improvement in MSE is gained by a new set of NP_x s. Then, the BP_x set is renewed by the new set of NP_x for the subsequent series of optimization. Simultaneously, the stp is reduced by a given reduction factor ($redFct$ of 1/4). The individual PS run is continued until the new stp becomes smaller than the critical stp ($crtstp$), which is set to $2\sim 10 \times 10^{-5}$ in the present study.

3.4. Selection of ionic currents for the optimization

When we get a new experimental record of AP, we do not start the analysis with an automatic optimization of G_x but first adjust the baseline model by conducting the conventional manual fitting. The nine ionic currents in Eq 1 in the baseline model are adjusted bit by bit to superimpose the simulated AP on the experimental one. During this step, it is important to pay attention to the influences of each sf_x adjustment on the simulated AP configuration on the computer display. Thereby, one may find several key current components which should be used in the automatic parameter optimization. Usually, currents showing a

Improved identifiability of cardiac AP model parameters by physiological constraints

9

relatively large magnitude of G_x were selected for the automatic optimization according to Eq 2, while those which scarcely modified the simulated AP were left as default values in the baseline model.

3.5. Principal component analysis of the cell-specific models

When the orp test is conducted with p elements, it is possible to record the final point BP where the MSE is improved in the p -dimensional space. Suppose we represent the matrix when n data points are acquired as an $n \times p$ matrix X . In that case, we obtain a vector space based on the unit vector that maximizes the variance (first principal component: PC1) and the p -dimensional unit vector orthogonal to it (loadings vector $\mathbf{w}_{(k)} = (w_1, w_2, \dots, w_p)$). It is possible to convert each row, $\mathbf{x}_{(i)}$ of the data matrix X into a vector of principal component scores, $\mathbf{t}_{(i)}$. The transformation is defined by

$$\mathbf{t}_{k(i)} = \mathbf{x}_{(i)} \cdot \mathbf{w}_{(k)} \text{ for } i = 1, 2, \dots, n \quad k = 1, 2, \dots, p \quad \text{Eq 9}$$

In order to maximize variance, the first weight vector $\mathbf{w}_{(1)}$ corresponding to the first principal component thus has to satisfy,

$$\mathbf{w}_{(1)} = \arg \max_{\mathbf{w}} \left\{ \frac{\mathbf{w}^T X^T X \mathbf{w}}{\mathbf{w}^T \mathbf{w}} \right\} \quad \text{Eq 10}$$

The k -th component can be found by subtracting the first $(k-1)$ -th principal components from X

$$\widehat{X}_k = X - \sum_{s=1}^{k-1} X \mathbf{w}_{(s)} \mathbf{w}_{(s)}^T \quad \text{Eq 11}$$

Then the weight vector is given as a vector such that the variance of the principal component scores is maximized for the new data matrix.

$$\mathbf{w}_{(k)} = \arg \max_{\mathbf{w}} \left\{ \frac{\mathbf{w}^T \widehat{X}_k^T \widehat{X}_k \mathbf{w}}{\mathbf{w}^T \mathbf{w}} \right\} \quad \text{Eq 12}$$

3.6. Membrane excitation and its cooperativity with intracellular ionic dynamics

When any of G_{xs} is modified, the intracellular ion concentrations ($[\text{ion}]_i$) change, although the variation is largely compensated for with time in intact cells through modification of the activities of both $3\text{Na}^+/2\text{K}^+$ pump (NaK) and $3\text{Na}^+/1\text{Ca}^{2+}$ exchange (NCX). In the present study, we imitated this long-term

Improved identifiability of cardiac AP model parameters by physiological constraints

10

physiological homeostasis of $[ion]_i$ by introducing empirical Eqs 13 and 14. These equations induced 'negative feedback' to the capacity ($maxI_{NaK}$ and $maxI_{NCX}$) of these ion transporters. Namely, each correcting factor (crf_x) was continuously scaled to modify the limiting activity of the transporters to keep the $[Na^+]_i$ or the total amount of Ca within the cell (Ca_{tot}) equal to their pre-set level ($stdNa_i$, $stdCa_{tot}$) with an appropriate delay (coefficients 0.3 and 0.008 in Eqs 13 and 14, respectively).

For the control of $[Na^+]_i$,

$$\Delta crf_{NaK} = -(stdNa_i - Na_i) \times 0.3, \quad stdNa_i = 6.1mM, \\ I_{NaK} = (crf_{NaK} \cdot maxI_{NaK}) \cdot vcy_{NaK} \quad \text{Eq 13}$$

For the control of Ca_{tot} ,

$$\Delta crf_{NCX} = -(stdCa_{tot} - Ca_{tot}) \times 0.008, \quad stdCa_{tot} = 79amol, \\ I_{NCX} = (crf_{NCX} \cdot maxI_{NCX}) \cdot (k_1 \cdot E_{1Na} \cdot E_{1NCX} - k_2 \cdot E_{2Na} \cdot E_{2NaCa}) \quad \text{Eq 14}$$

The Ca_{tot} is given by $[Ca]_i$ included in the cytosolic three Ca-spaces *jnc*, *iz*, and *blk*, and in the sarcoplasmic reticulum SR_{up} and SR_{rl} in the free or bound forms, respectively.

$$Ca_{tot} = [Ca_{tot}]_{jnc} \cdot vol_{jnc} + [Ca_{tot}]_{iz} \cdot vol_{iz} + [Ca_{tot}]_{blk} \cdot vol_{blk} + [Ca_{tot}]_{SR_{up}} \cdot vol_{SR_{up}} + [Ca_{tot}]_{SR_{rl}} \cdot vol_{SR_{rl}} \quad \text{Eq 15}$$

Here, the *vol* is the volume of the cellular Ca compartment (see more detail, [11]).

4. Results

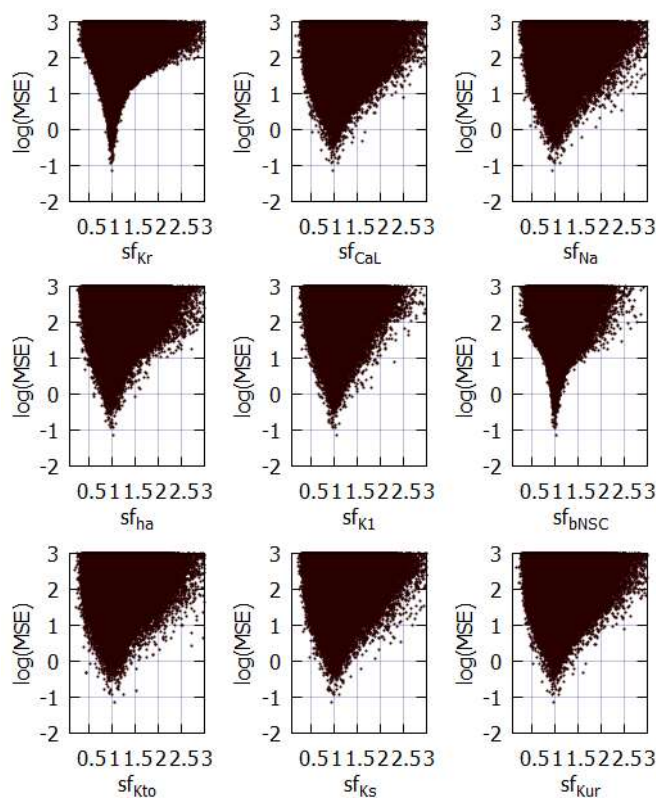
4.1. Mapping the magnitude of MSE over the nine global parameter space

Parameter identifiability has been one of the central issues in the parameter optimization of biological models [14,20]. For confirmation of the identifiability of a unique set of solutions using the parameter optimization method, mapping of the MSE distribution is required over an enlarged parameter space defined by the sf_x of the nine ionic currents of the baseline model. The randomization of sf_x ranged from 1/10 to ~ 10 times the default values, and the calculation was performed for ~5,000,000 sets, as shown in Fig 1, where magnitudes of $\log(MSE)$ were plotted against each sf_x on the abscissa.

Improved identifiability of cardiac AP model parameters by physiological constraints

11

The data points of MSE at a given sf_x include all variable combinations of the other eight sf_x s. The algorithm of the PS method searches for a parameter set, which gives the minimum MSE at a given stp through the process of optimization. Although drawing a clear envelope curve by connecting the minimum MSEs at each sf_x was difficult because of the insufficient number of data points in these graphs (Fig 1), an approximate envelope of the minimum MSEs may indicate a single global minimum of MSE located at the control sf_x



equals one, as typically exemplified by I_{Kr} - and I_{bNSC} -MSE relations. On both sides of the minimum, steep slopes of MSE/sf_x are evident in all graphs. Outside this limited sf_x -MSE area, the global envelope showed a gentle and monotonic upward slope toward the limit on the right side. No local minimum was observed in all of the sf_x -MSE diagrams except the central sharp depression. It was concluded that the theoretical model of cardiac membrane excitation (hVC model) has only a single central sharp depression corresponding to the control model parameter.

Fig 1. Distribution of MSE calculated between the target and the simulated APs modified by randomizing the sf_x of 9 ionic currents in the coordinates of MSE- sf_x . All MSE data points were plotted on the logarithmic ordinate against the linear sf_x . A total of 5,141,382 points were calculated in cell model No.86 over the range of $1/10 \sim 10$ times the default sf_x . Since the configuration of V_m records were largely unrealistic at $sf_x > 3$, MSE points were cut out over $sf_x > 3.0$. To demonstrate the sharp decrease in MSE, the data points were densely populated near the default sf_x .

4.2. The prompt necessity for a method of parameter optimization as indicated by hiPSC-CM APs

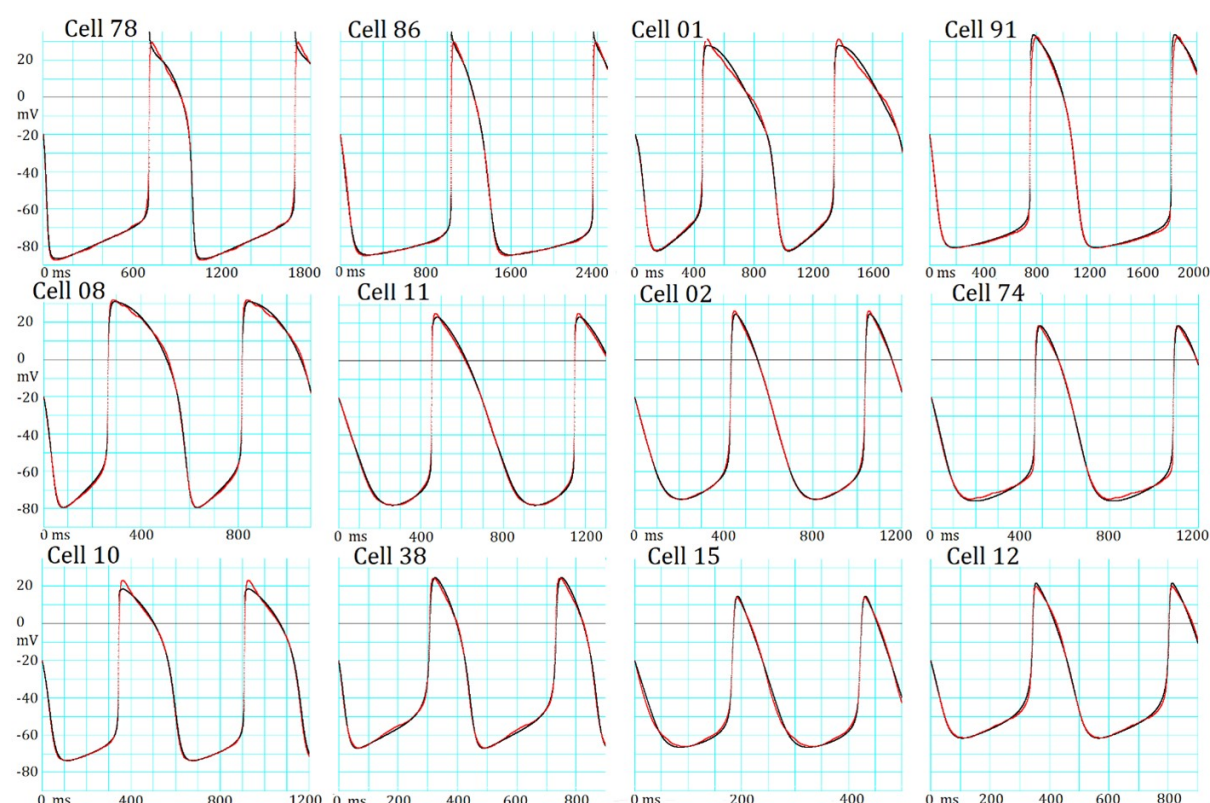
Fig 2 illustrates records of spontaneous APs (red traces) obtained in 12 experiments in the sequence of MDP (See Supplemental Materials for detail). All experimental records were superimposed with the simulated AP traces (black traces) obtained by the conventional manual fitting. In most cases, MSE of $1 \sim 6 \text{ mV}^2$

Improved identifiability of cardiac AP model parameters by physiological constraints

12

remained (Eq 7) at the end of the manual fitting. This extra component of MSE might be largely attributed to slow fluctuations of V_m of unknown origin in experimental recordings because the non-specific random fluctuations were quite different from the exponential gating kinetics of ion channels calculated in mathematical models. This extra-noise seriously interfered with the assessment of the accuracy of the parameter optimization of G_x in the present study. Thus, APs produced by the manual adjustment ('cell specific model') was used as the target AP, which were completely free from the extra noise when examining the feasibility of the parameter optimization algorithm.

A comparison of AP configurations between these hiPSC-CMs clearly indicated that the classification of these APs into atrial-, ventricular- and nodal-types was virtually impractical, as described in [7]. On the other hand, if provided with the individual models fitted by an objective parameter optimizing tools using the baseline model (black trace), the results should be fairly straightforward not only in estimating the functional expression level of ion channels but also in clarifying the role of each current system or the ionic mechanisms in generating the AP configuration in a quantitative manner. Thus, the objective parameter optimization of the mathematical model is a vital requirement in cardiac electrophysiology.



Improved identifiability of cardiac AP model parameters by physiological constraints

13

Fig 2. The manual fitting of variable AP configurations in 12 different hiPSC-CMs. Each panel shows the experimental record (red) superimposed by the model output (black) of the baseline model adjusted by the conventional manual fitting. At the top of each pair of AP records, the experimental cell number is presented. The extra fluctuations are obvious during the AP plateau in Cells 78, 08 and 01, while in Cells 15 and 74 during SDD. The length of abscissa is markedly different to illustrate the interval between two successive peaks of AP.

Table 1. AP metrics and MSE calculated after the manual fitting of varying AP configurations in 12 different hiPSC-CMs in Fig 2.

Table 1 indicates the AP metrics; the cycle length (CL), the peak potential of the plateau (OS), the maximum diastolic potential (MDP), and the AP duration measured at -20 mV in addition to the MSE between individual experimental record and the model output fitted by manual fitting. The CL, MDP and AP were very variable among different AP recordings of cells shown in Fig 2. The cells were arranged by the sequence of MDP.

	CL (ms)	OS (mV)	MDP (ms)	APD(ms) at -20mV	MSE (mV ²)
Cell 78	983.8	29.6	-87.4	271.7	5.8443
Cell 86	1326.0	29.7	-85.0	289.2	4.0554
Cell 01	887.4	31.2	-82.2	435.0	3.9330
Cell 91	1058.0	33.0	-80.4	308.6	7.2156
Cell 08	551.4	32.0	-79.5	287.6	1.4043
Cell 11	695.0	25.3	-77.6	243.5	2.6683
Cell 02	603.9	26.4	-74.9	173.4	1.0412
Cell 74	622.8	18.5	-74.8	157.0	2.2589
Cell 10	564.3	23.0	-73.7	220.9	3.2194
Cell 38	425.4	24.2	-66.8	123.4	3.6626
Cell 15	239.5	13.8	-66.1	57.1	2.8607
Cell 12	458.6	19.7	-61.5	119.0	1.3514

Table 1 indicates the AP metrics; the cycle length (CL), the peak potential of the plateau (OS), the maximum diastolic potential (MDP), and the AP duration measured at -20 mV in addition to the MSE between individual experimental record and the model output fitted by manual fitting. The CL, MDP and AP were very variable among different AP recordings of cells shown in Fig 2. The cells were arranged by the sequence of MDP.

The experimental study using the hiPSC-CMs was approved by the Kyoto University ethics review board (G259) and conformed to the principles of the Declaration of Helsinki.

Improved identifiability of cardiac AP model parameters by physiological constraints

14

4.3. Feasibility of the PS algorithm for parameter optimization of membrane excitation models

The automatic parameter optimization was applied to the model of cardiac membrane excitation in a limited number of studies (for review, see [23,26,35,36]) using various optimization methods, such as genetic algorithms. To the best of our knowledge, the principle PS algorithm has not been successfully applied to the detailed mathematic models of cardiac membrane excitation composed of both ionic channel and ion transporters models, except for the pioneering work in [12], which applied more general gradient-based optimization method to the simple ventricular cell model of Beeler and Reuter (BR model)[37].

Fig 3 shows a typical successful run of the new PS method in a hiPSC-CM, which showed an MDP of ~ 85 mV. The PS parameter optimization was started after randomizing the sfs s of the major six currents, I_{Kr} , I_{CaL} , I_{Na} , I_{ha} , I_{K1} and I_{bNSC} , in the manual fit model within a range of $\pm 15\%$ around the default values (normalized magnitude of 1). Fig 3A-1~3 compares the simulated $V_{m,orp}$ (black) with the target $V_{m,t}$ (red) at the repeat number $N=1$, 50 and 1167, respectively (Eq 8). The OS, APD as well as the CL of spontaneous AP were markedly different at the first cycle of AP reconstruction (Fig 3A-1). These deviations were largely decreased at the PS cycle (Fig 3A-2 V_m , at $N = 50$), and became invisible in the final result (Fig 3A-3, $N = 1167$). The final individual current flow of nine current components are demonstrated in the lower panel of Fig 3A-3 (I_m).

Improved identifiability of cardiac AP model parameters by physiological constraints

15

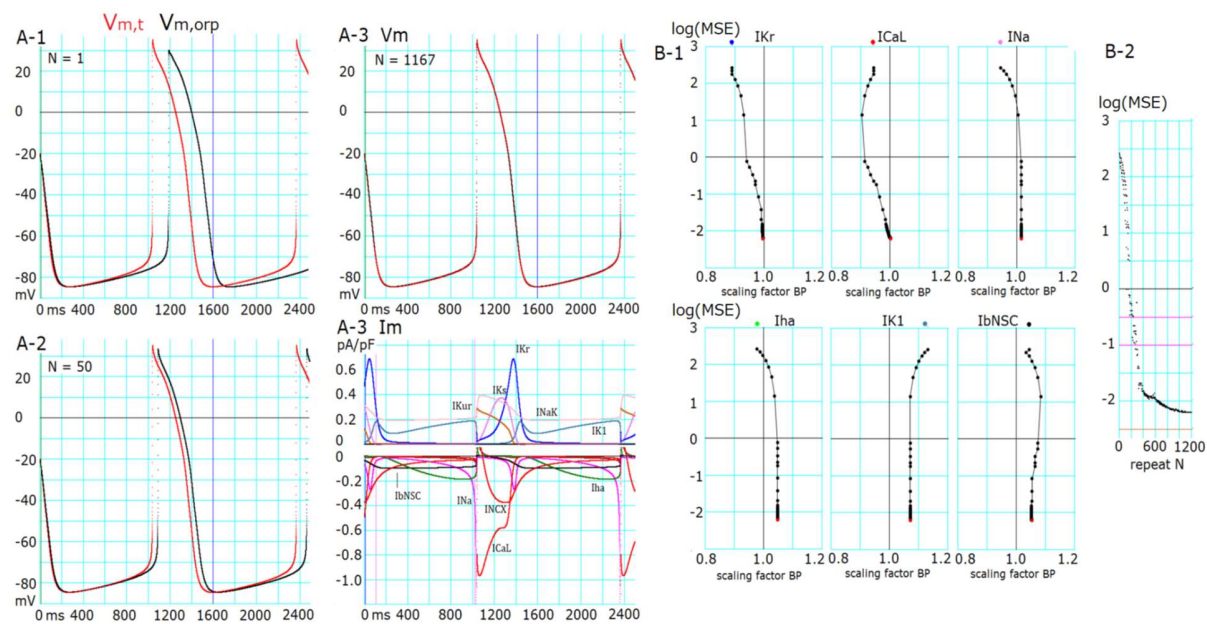


Fig 3. Results of the successful optimization in a cell (Cell86).

(A-1) Target AP ($V_{m,t}$, red) and AP generated by randomized initial sf_x s ($V_{m,orp}$, black). (A-2) $V_{m,t}$ (red) and $V_{m,orp}$ (black) generated after 50 cycles of adjusting BP. (A-3) V_m : $V_{m,t}$ (red) and $V_{m,orp}$ (black) generated by the final sf_x s. I_m : corresponding time courses of each current for the finalized AP shown in A-3 V_m . (B-1) Changes in sf_x s vs. $\log(MSE)$ during a successful optimization process of PS. (B-2) $\log(MSE)$ of all BP points during the search process in PS. The initial values of sf_x s are plotted by corresponding colors at the top of each sf_x - $\log(MSE)$ graph.

The time course of decreasing $\log(MSE)$ evoked by the multi-run PS optimization is plotted for each sf_x in Fig 3B-1 every time of resetting the set of base points. Fig 3B-2 shows all of the $\log(MSE)$ obtained at every adjustment by stepping individual BP points. The movement of all sf_x s were synchronized to decrease $\log(MSE)$ from ~ 2.4 to 1 during the initial 180 cycles of decreasing $\log(MSE)$, but the search directions of BP were quite variable. The detailed adjustment of sf_x s below $\log(MSE) < 0$ was driven by adjusting I_{Kr} , I_{CaL} and I_{bNSC} in this cell. The values of sf_{Kr} , sf_{CaL} and sf_{Na} approached the correct value of 1, while those for I_{ha} , I_{K1} and I_{bNSC} remained deviated from the unit by less than 10% of the value. The explanation for the deviation of these three sf_x s from the unit will be examined in the next section of the Results.

Improved identifiability of cardiac AP model parameters by physiological constraints

16

4.4. The six-parameter orp test successfully determined the conductance parameters of membrane excitation models

In individual runs, the PS optimization was frequently interrupted at intermediate levels during the progress of optimization and the probability of reaching $\log(MSE)$, for example, below -2, rapidly decreased with increasing extent of the randomization of the initial set of parameters. Moreover, the complementary relations between several ionic currents in determining dV_m/dt might have hampered the parameter optimization. These facts indicate the requirement of statistical measures to improve the accuracy of the PS method. Fig 4 shows the results of orp tests, in which the optimization shown in Fig 3 was repeated several hundred times, and all results were plotted in a common coordinate of $\log(MSE)$ and individual sf_x s. The population of sf_x correctly converged at a single peak point very close to 1 with increasing negativity of $\log(MSE)$ for sf_{Kr} , sf_{CaL} , and sf_{Na} , while sf_{ha} , sf_{KI} , and sf_{bNSC} showed obvious variance. Nevertheless, they also showed a clear trend toward convergence to 1 in the average.

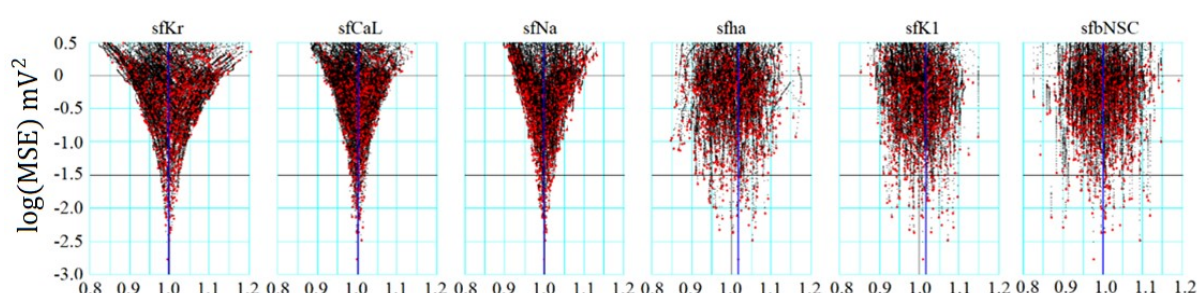


Fig 4. Convergence of sf_x in the orp test for Cell86. The ordinate is the $\log(MSE)$ and the abscissa is the normalized amplitude of sf_x ; x stands for Kr , CaL , Na , ha , KI , and $bNSC$. Black points were obtained in the progress of optimization, and red ones are the final points in 829 runs of PS optimization.

Table 2 summarizes the mean of sf_x determined for the top 20 runs of the PS parameter optimization in each of the 12 cells illustrated in Fig 2. The $[Na^+]_i$ as well as Ca_{tot} was well controlled to the reference levels (std_{Nai} , and std_{Cator} in Eqs 16 and 17) of 6.1 mM and 79 amol, respectively, at the end of the parameter optimization to ensure the constant $[Na^+]_i$ as well as Ca_{tot} . The mean of final $\log(MSE) = -2.74$ indicates that the MSE was reduced by five orders of magnitude from the initial level just after the randomization by the orp test, like in the successful example shown in Fig 3B. The mean of individual sf_x s were very close to 1 with

Improved identifiability of cardiac AP model parameters by physiological constraints

17

a minimum standard error (SE) of mean, which were less than 1% of the mean, even for I_{K1} , I_{bNSC} and I_{ha} , which showed weak convergence against $\log(MSE)$. These results well validate the accuracy of the parameter optimization using the multi-run PS method in all of 12 cell-specific models, which showed the large variety of spontaneous AP recorded in the hiPSC-CMs.

Table 2. Measurements of sf_x s (mean + SE, n = 20), $[Na^+]_i$, mM and Ca_{tot} in amol in the 12 cells.

Cell No.	log(MSE)	sfKr	sfK1	sfCaL	sfbNSC	sfha	sfNa	sfKur	$[Na^+]_i$ (mM)	Ca_{tot} (amol)
78	-2.48321	1.00005	1.00157	1.00037	0.99460	1.00060	1.00134		6.10550	78.99979
91	-2.42008	0.99952	1.00644	1.00063	1.00280	1.00470	1.00068		6.09977	79.00044
86	-2.80257	1.00166	1.01394	1.00142	1.02670	1.00253	1.00702		6.09466	79.00008
01	-2.79709	0.99871	1.00157	0.99756	0.99692	1.00054	0.99779		6.08973	78.99984
08	-3.07432	0.00094	0.99982	1.00088	1.00041	0.99968	0.99985		6.12201	79.00056
11	-2.67641	1.00186	1.00686	1.00129	0.99768	1.00253	1.01028		6.10385	78.99995
10	-1.70278	1.00322	1.01081	1.00424	1.00396		0.99883		6.10968	79.00018
02	-2.35441	1.00161	1.02038	1.00341	0.99815	1.01324	1.00954		6.10184	79.00004
74	-2.43399	1.00126	1.01838	1.00308	0.99898	1.00004	1.00435		6.10118	79.99979
38	-3.01883	1.00075		1.00106	1.00061		0.98866	1.00151	6.10530	78.99969
15	-3.85992	1.00003		0.99894	0.99996		1.00015	0.98653	6.09902	79.00022
12	-3.33037	0.99978		1.00030	0.99990	0.97587		1.00188	6.10012	79.00007
Ave	-2.74617	0.99992	1.00886	1.00110	1.001723	0.99997	1.001681	0.99664	6.10272	79.08339
SE	0.07065	0.00093	0.010000	0.00164	0.00430	0.00729	0.00544	0.00690	0.00017	0.000345

The top 20 results obtained in the multi-run orp method were analyzed in each cell. Grand average (Ave) and SE are listed at the bottom rows.

4.5. Complementary relationship among I_{K1} , I_{ha} and I_{bNSC}

Fig 5A illustrates the distribution of sf_x s amplitude in the top 20 data points, where the final sf_x s in individual runs were connected with lines for each run of PS in Cell 86 (Fig 2). The values of standard error (SE) of mean were quite small in the sf_{Kr} and sf_{CaL} , less than 1%. In contrast, sf_{ha} , sf_{K1} and sf_{bNSC} showed evidently larger deviations. This finding is interesting since the former currents are mainly involved in determining the AP configuration and the latter group mainly in driving the relatively long-lasting SDD of approximately 1 sec in duration.

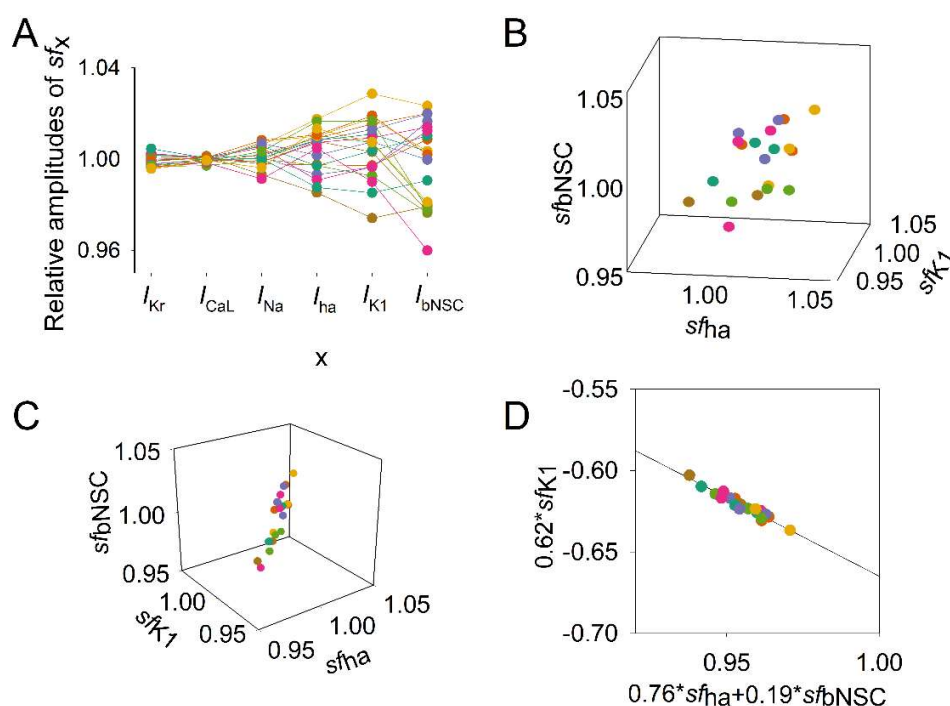
Improved identifiability of cardiac AP model parameters by physiological constraints

18

Thus, we analyzed the distribution of sf_{ha} , sf_{K1} and sf_{bNSC} within the top 20 MSE. Fig 5B and C show the distribution of sf_x points in the space of the three sf_x dimensions. In Fig 5B, the 20 data points seemed to be dispersed randomly in the parameter space, but when the space was rotated to a specific angle, a linear distribution was observed as in Fig 5C, indicating that the points are distributed approximately on a plane surface in the 3D space. Using the multiple regression analysis, we could obtain an equation that fits the 20 data points as follows ($R^2=0.872$);

$$0.762 \cdot sf_{ha} - 0.619 \cdot sf_{K1} + 0.191 \cdot sf_{bNSC} = 0.333554 \quad Eq\ 16$$

By replotting the data points in the 2D space with the abscissa for the sum of two inward-going currents ($0.76 sf_{ha} + 0.19 sf_{bNSC}$) and the ordinate for the outward current $0.62 sf_{K1}$, we obtained a regression line as shown in Fig 5D. The close correlations among the three sf_x s were indicated with a quite large R^2 of 0.941. This finding well confirms that the three currents have complementary relations with each other to give virtually identical configurations of spontaneous AP. In other words, $\log(MSE)$ remains nearly constant as far as the composition of the currents satisfies the relationship given by Eq 16.



Improved identifiability of cardiac AP model parameters by physiological constraints

19

Fig 5. Distribution of sf_x within the top 20 sets of sf_x s obtained from the multi-run orp test in Cell86 in Fig 2. Data points of normalized sf_x in each set were depicted in a different color. (A) amplitudes of each sf_x (indicated on the abscissa) were plotted. (B) Three parameters, sf_{ha} , sf_{K1} , and sf_{bNSC} were plotted in the 3D plot. (C) A different solid angle view of the 3D plot showed a linear correlation; see text for the plot in (D)

The complementary relationship was further examined by conducting the orp test after fixing one of the two factors, sf_{K1} or $(sf_{ha} + sf_{bNSC})$, illustrated in Fig 5B. Fig 6A shows the $\log(MSE)$ vs. sf_{K1} relation when the $(sf_{ha} + sf_{bNSC})$ were fixed at the values obtained by the orp test. Indeed, the typical convergence of the sf_{K1} was obtained. Alternatively, if the sf_{K1} was fixed, the convergence was obviously improved for both sf_{ha} and sf_{bNSC} (Fig 6B-1, 2), but it was less sharp if compared to sf_{Kr} , sf_{CaL} and sf_{Na} (not shown, but refer to corresponding results in Fig 4A). This finding was further explained by plotting the relationship between the two inward currents, I_{ha} and I_{bNSC} , as illustrated in Fig 6C. The regression line for the data points was fitted by Eq 17 with $R^2 = 0.86$, supporting the complementary relationship between the two inward currents, I_{ha} and I_{bNSC} .

$$0.9736 \cdot sf_{bNSC} + 0.2281 \cdot sf_{ha} = 1.2024 \quad Eq\ 17$$

The moderately high R^2 indicates that the SDD is determined not only by the major I_{ha} and I_{bNSC} but also by other currents, such as I_{K1} , I_{Kr} , the delayed component of I_{Na} (I_{NaL}) and I_{CaL} , which were recorded during the SDD as demonstrated in Fig 3.

Essentially the same results of complementary relationship among sf_{ha} , sf_{bNSC} and sf_{K1} were obtained in Cell 91, which also showed the long-lasting SDD with the very negative MDP as in Cell 86, as shown in Fig 2 and Table 2. The regression relation for the data points was fitted by Eqs 18 and 19 with $R^2 = 0.656$ and 0.472, respectively.

$$0.572 \cdot sf_{ha} - 0.132 \cdot sf_{K1} + 0.810 \cdot sf_{bNSC} = 1.25891 \quad Eq\ 18$$

$$0.9279 \cdot sf_{ha} + 0.3706 \cdot sf_{bNSC} = 1.30025 \quad Eq\ 19$$

Improved identifiability of cardiac AP model parameters by physiological constraints

20

414

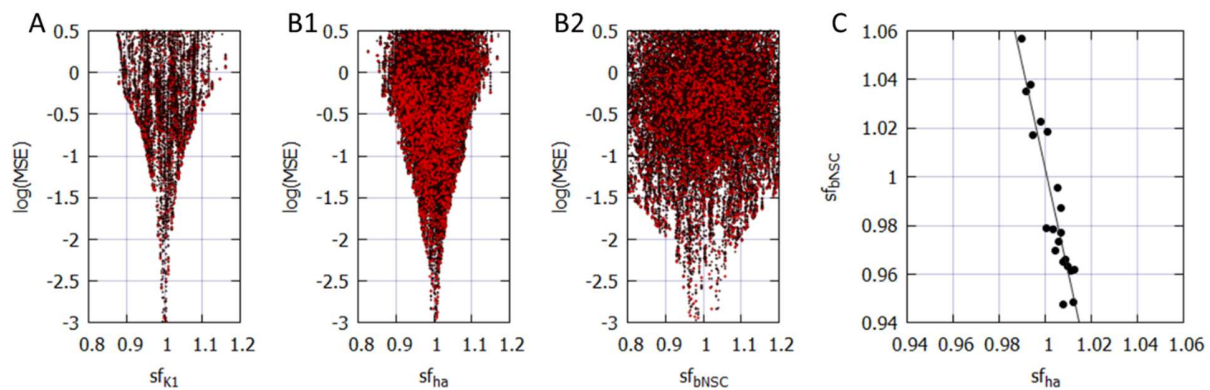


Fig 6. The complementary relations among sf_{k1} , sf_{ha} and sf_{bNSC} .

(A) and (B) results of the multi-run orp test. A; the perfect convergence of sf_{k1} when sf_{ha} and sf_{bNSC} were fixed. (B1) improved convergence of sf_{ha} and (B2) sf_{bNSC} when sf_{k1} was fixed. In these two orp tests, sf_x of other currents showed quite comparable convergence as in Fig 4A. (C) the correlation between sf_{ha} and sf_{bNSC} .

4.6. Principal components in the hiPSC-CM model

The PS frequently got stuck during the progress of parameter optimization and failed to reach the global minimum in the present study (Figs 4 and 6). The major cause of this interruption may most probably be attributed to the fact that sf_x s were used directly as the search vector of the PS. In principle, the algorithm of PS parameter optimization gives the best performance when the parameters search is conducted in orthogonal dimensions where each dimension does not affect the adjustment of other sf_x [28]. To get deeper insights, we applied the principal component (PC) analysis to the set of 6 sf_x s selected in the baseline model. We performed PC analysis on the data points recorded in the vicinity of the minima (using the top 20 data).

As illustrated in Fig 7, each of the 6 PCs was not composed of a single sf_x but mostly included multiple sf_x sub-components. This finding indicates the inter-parameter interactions during the process of parameter optimization. For example, the changes in sf_{k1} or sf_{bNSC} simultaneously affect PCNo.1, 3, 6 or 1, 2, 3 PCs, respectively. Both sf_{CaL} and sf_{Kr} affect PCNo.4, 5. It might be concluded that the frequent interruptions of PS parameter optimization are most probably caused by the sporadic appearance of the local minima of MSE through interactions among sf_x s.

Improved identifiability of cardiac AP model parameters by physiological constraints

21

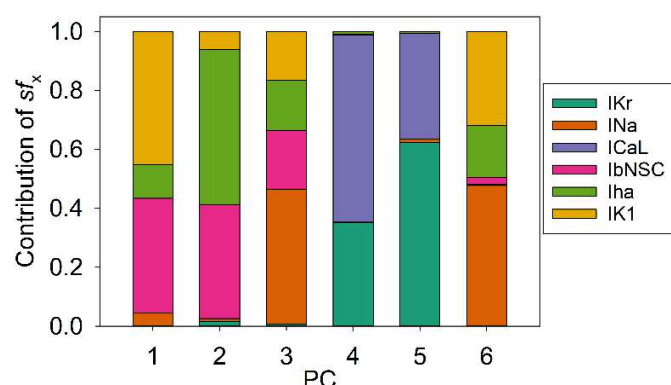


Fig 7. PC1~6 to describe distribution of the 6 sf_x s. PC analysis was performed on the data population of the top 200 runs of the orp test as in Fig 4, which showed good optimization results (Cell 86). Each magnitude of 6 PCs was normalized to give a unit magnitude. Note each PC is composed of multiple components of ionic current, which are indicated in the Index with corresponding colors.

5. Discussion

New findings in the present study are listed below.

- (1) Mapping the MSE distribution over the enlarged parameter space was conducted by randomizing the G_x s of the baseline model. It was confirmed that the baseline model has only a single sharp depression of MSE at the default G_x s (Fig 1).
- (2) The preliminary cell-specific models were firstly prepared by the conventional manual tuning of G_x s to superimpose the model output on each of twelve experimental AP recordings (Fig 2). Thereby, the parameter search space was restricted to a relatively small space to facilitate parameter optimization.
- (3) The sf_x s of 4 ~ 6 G_x parameters were initially assigned random values from a uniform distribution ranging between $\pm 10\%$ of default values. The MSE was calculated between the randomized model output and the intact model AP as the target of optimization (Fig 3).
- (4) Plotting parameter sf_x in a common sf_x - MSE coordinates during each run of several hundred runs of optimization (Fig 4), we found that the sf_x distribution of IK_r , ICa_L , and INa converged sharply to

Improved identifiability of cardiac AP model parameters by physiological constraints

22

a single point with decreasing MSE, which exactly equaled the default ones. On the other hand, estimates of sf_{K1} , sf_{ha} and sf_{bNSC} deviated slightly within a limited range around the default values in cells showing long-lasting SDD (Fig 4).

- (5) For statistical evaluation, the mean \pm SE of sf_x in the top 20 estimates of MSE was calculated in individual cells (Table 2). The results of the parameter optimization in the 12 cells definitely indicated that the means of sf_{xs} were very close to 1.00, with the SE less than 0.01 for all G_{xs} .
- (6) A complementary relationship was found between sf_{K1} , sf_{ha} and sf_{bNSC} in determining the gentle slope of long-lasting SDD in two representative cells (Fig 5). Supporting this view, the sf_{K1} clearly focused on the unit provided that sf_{ha} and sf_{bNSC} were fixed and vice versa (Fig 6).
- (7) The six search vectors of sf_x of the presented model could be replaced by the same number of theoretical PCs, and each PC was mostly composed of multiple sf_{xs} (Fig 7). This finding definitely supports the view [12] that the complex interactions among I_{xs} might interrupt the progress of the parameter optimization when sf_{xs} were used as the search vector instead of using theoretical orthogonal ones.

The use of an initial randomized set of parameters was crucial in examining if an optimization method can determine unique estimates independent from the initial set of parameters, as used in the GA-based method for determining the G_{xs} of the mathematical cardiac cell model [23]. The findings listed above well confirmed the feasibility of the PS method. Most probably, the PS method is applicable to variable mathematical models of other cell functions as well. See [26] for a more systematic review of the parameter optimization in the cardiac model development.

It has been suggested that different combinations of parameters may generate simple outputs that are very similar [12,23–25]. In the present study, this notion may be explained at least in part by the complementary relationship, for example, between the I_{K1} , I_{ha} and I_{bNSC} in determining dV_m/dt of SDD, which is a function of the total current (Eq 2, Figs 5 and 6). The gradient-based optimization method relies on the precise variation in the time course of dV_m/dt induced by the time-dependent changes in individual sf_{xs} (Eq 2).

Improved identifiability of cardiac AP model parameters by physiological constraints

23

Therefore, the MSE was calculated over the whole time course of the spontaneous APs. Note, we did not use the AP metrics, which reflect only indirectly the kinetic properties of individual currents. Even with this measure of calculating the MSE, the time-dependent changes in pO (Eq 3) might be relatively small between two major currents, I_{K1} and I_{ha} , in comparison to I_{bNSC} , which has no V_m -dependent gate during the SDD as shown in the current profile Fig 3A-3. We assume that the gradient-based optimization method will be able to determine different contributions of individual currents if the optimization is conducted only within a selected time window of SDD. If MSE is calculated over multiple phases of the spontaneous AP, the influence of a particular phase on the MSE should be diluted. In our preliminary parameter optimization, this problem was partly solved by using a weighted sum for different phases of the spontaneous AP in summing up the MSE.

The small amplitude of a given current might be an additional factor in the weak convergence of sf_x observed in the diagram of sf_x - MSE in the orp test of optimization. If the current amplitude was much smaller in reference to the sum of all currents in determining dV_m/dt (Eq 2), the resolution of the PS method would get lower. Sarkar et al. [24] demonstrated that the model output, for example, the AP plateau phase were almost superimposable when the different ratio of G_{Kr} and G_{pK} were used in reconstructing the model output (Figure 1 in [24]). They described that the AP metrics used for comparisons, such as APD, OS and APA seemed quite similar. It should be noted, however, that the results were obtained by applying different combinations of sf_x to the same TNNP model [33]. This means that the relative amplitudes of I_{Kr} and I_{pK} in the TNNP model were much smaller than the major I_{CaL} during the AP plateau, even though I_{Kr} and I_{pK} have totally different gating kinetics. Thus, the results of parameter optimization should be model-dependent. The same arguments will also be applied to the use of FR guinea pig model [38] in the study by Groenendaal et al. [23].

The gradient-based parameter optimization method was applied to the cardiac model of membrane excitation in [12], which analyzed the classic BR model [37]. The whole cell current in the BR model was composed of a minimum number of ionic currents, a background I_{K1} , and three time-dependent currents; I_{Na} , I_s , and I_{x1} , which were dissected from the voltage clamp experiments by applying the sucrose gap method to the multicellular preparation of ventricular tissue. The gatings of the latter three currents were formulated according to the Hodgkin-Huxley type gating kinetics, which was quite simple if compared with the recent

Improved identifiability of cardiac AP model parameters by physiological constraints

24

detailed description of the ionic currents. They described that the parameter optimization was difficult if the AP configuration was used as the target of the parameter optimization, and they used the time course of the whole cell current as of the target of parameter optimization. However, the number of parameters was quite large, 63 in total, including limiting conductances and the gating kinetics. They suggested the feasibility of the parameter optimization method will be improved if provided with additional experimental data.

In the modern mathematical cardiac cell models, most ionic currents were identified by the whole-cell voltage clamp and single channel recordings in dissociated single myocyte [39] using the patch clamp technique [40] and by identifying their molecular basis of membrane protein. It has been clarified that the molecular basis of the ion channels expressed in the hiPSC-CMs is mostly identical to those in the adult cardiac myocytes rather than in the fetal heart (GSE154580 GEO Accession viewer (nih.gov)). Moreover, the gating kinetics have been much detailed to characterize the ionic currents within the cell model. In principle, the detailed characterization of individual currents should facilitate the identifiability of the model parameter but should not necessarily interfere with parameter optimization. We consider that the manual fitting of the model parameters to the AP recording by using a priori knowledge of biophysical mechanisms should largely facilitate the subsequent automatic parameter optimization. It might also be noted that the ionic currents left at the default values work as a kind of constraint to improve the identifiability of the target parameters.

After validating the automatic parameter optimization method, the final goal of our study is to find the principle of ionic mechanisms, which are applicable to the full range of variations of spontaneous AP records in both hiPSC-CMs and matured cardiomyocytes. For this purpose, we will apply the multi-run PS method to the experimental AP recordings using the initial parameter sets obtained by the conventional manual fit. The protocol of measuring the G_{Ks} will be the same as used in the present study except for the use of experimental AP recordings in place of the output of the 'cell-specific model'. In our preliminary analysis, the magnitude of individual model parameters obtained by the manual tuning was corrected by less than ~15% by the objective parameter optimization. Finally, the ionic mechanisms underlying the SDD of variable time courses will be analyzed in a quantitative manner, for example, by using the lead potential analysis [41], which explains changes in V_m in terms of G_x of individual currents.

Improved identifiability of cardiac AP model parameters by physiological constraints

25

Limitations

In general, obvious limitations of the mathematical models of cardiac membrane excitation so far published are caused by a shortage of functional components inherent in intact cells. For example, the $[ATP]_i$ controlled by energy metabolism is a vital factor in maintaining the physiological function of ion channels as well as the active transport Na^+/K^+ pump [42]. Moreover, the followings are still not implemented in most models; the modulation of the ion channel activity through phosphorylation of the channel proteins, detailed modulation of the channel by the $[Ca^{2+}]_i$, the alterations of ion channel activity by PIP_2 [43,44] and by the tension of the cell membrane through the cell volume change [45–48]. The detailed Ca^{2+} dynamics of the $[Ca^{2+}]_i$ are still not implemented in most of the cardiac cell models; such as the Ca^{2+} release from SR activated through the coupling of a few L-type Ca^{2+} channels with a cluster of RyRs at the dyadic junction [49], the Ca^{2+} diffusion influenced by the Ca^{2+} -binding proteins [50]. To simulate the Ca^{2+} -binding to troponin during the development of the contraction, it is necessary to include a dynamic model of contracting fibers [51–54]. These limitations should be thoroughly considered when pathophysiological phenomena, such as arrhythmogenesis are concerned. The scope of the present study is limited to the AP configurations of hiPSC-CMs, which were assumed to be 'healthy' with respect to the above concerns; for example, $[ATP]_i$, $[Na^+]_i$ and Ca_{tot} were kept constant, and the standard contraction model was implemented as in the hVC model.

The parameter optimization presented in this study could be achieved in a practical way by limiting the number of unknown parameters. We determined only $G_{x,s}$ based on the assumption that ion channel kinetics are preserved as the same in the hiPSC-CMs as in the matured myocytes. Usually, 4~6 ionic currents were selected for the optimization. We found that the orp method could be performed simultaneously for all nine ionic currents described in Eq 1. However, the computation time was radically prolonged, and the resolution was not as high as obtained by using the modest number of parameters. We consider that the determination of the limited number of $G_{x,s}$ is quite relevant to solving physiological problems in terms of detailed model equations for each current system.

Improved identifiability of cardiac AP model parameters by physiological constraints

26

Although I_{NCX} and I_{NaK} contribute sizeable fractions of the whole-cell outward and inward currents, respectively (Fig 3A-3), we excluded the scaling factors, sf_{NaK} and sf_{NCX} from the parameter optimization for the sake of simplicity. Instead, the possible drift of the intracellular ion concentrations was virtually fixed during the repetitive adjustment of ionic fluxes by varying sf_x as shown in Table 2. The introduction of the empirical equations (Eqs 13 and 14) was quite useful to adjust the $[Na^+]_i$ and Ca_{tot} (Table 2) so that the time course as well as magnitude of I_{NCX} remained almost constant during the parameter optimization. When influences of varying $[Na^+]_i$ and/or Ca_{tot} are examined under various experimental conditions in future, the reference levels of $[Na^+]_i$ and/or Ca_{tot} ($stdNai$ and $stdCatot$ in Eqs 13 and 14) might be replaced by experimental measurements.

The parameter optimization method was not applied to several ionic currents. For example, it was difficult to determine the kinetics of T-type Ca^{2+} channel (I_{CaT} ; Cav 3.1) and excluded in the present study. A very fast opening and inactivation rates described in [55] suggest a complete inactivation of I_{CaT} over the voltage range of SDD, while a sizeable magnitude of window current described in [56] suggests a much larger contribution to SDD. The kinetics of I_{CaT} still remain to be clarified in experimental examinations. The sustained inward current, I_{st} , is recently attributed most probably to the Cav 1.3 [57], which is activated at a more negative potential range than the activation of I_{CaL} (Cav 1.2) [58,59]. The I_{bNSC} was used to represent net background conductance in the present study. However, several components of the background conductance have been identified on the level of molecular basis in matured myocytes (see for review TRPM4, [60]). Experimental measurements of the current magnitude for each component are also awaited.

Gábor and Banga indicated that the multi-run method had shown good performance in certain cases, especially when high-quality first-order information is used and the parameter search space is restricted to a relatively small domain [16] (see also [19]). Indeed, the manual fitting of the parameters (Fig 1) was required to utilize the presented multi-run PS method over the restricted search space. One of the major difficulties in the manual fitting of individual G_x s arose during the SDD, where I_{Kr} , I_{K1} , I_{bNSC} , and I_{ha} , in addition to I_{NaK} and I_{NCX} constitute the whole-cell current (Fig 3A-3). Close inspection of the current components (Fig 3A-3), however, suggests hints of how to do with the manual fit. The transient peak of I_{Kr} dominates the current profile during the final repolarization phase from -20 to -60 mV in all 12 hiPSC-CMs [61], since I_{CaL} and I_{Ks}

Improved identifiability of cardiac AP model parameters by physiological constraints

27

rapidly deactivated before repolarizing to this voltage range. The I_{NaK} and I_{NCX} are well controlled by the extrinsic regulation in Eqs 13 and 14. Thus, the manual fitting of sf_{Kr} is firstly applied to determine sf_{Kr} . The MDP more negative than -70 mV is adjusted by the sum of time-dependent ($I_{Kr} + I_{K1}$) and the time-independent I_{bNSC} . Then, I_{Kr} is deactivated when depolarization becomes obvious after the MDP, and gradual activation of I_{ha} and the depolarization-dependent blocking of I_{K1} by the intracellular substances [62] take the major role in promoting the initial linear phase of SDD. Thus, the amplitude of sf_{K1} and sf_{bNSC} might be approximated during the initial half of SDD. The late half of SDD, including the foot of AP, namely the exponential time course of depolarization toward the rapid rising phase of AP, is mainly determined by the subthreshold V_m -dependent activation of I_{Na} (after MDP more negative than -70 mV) and/or I_{CaL} (after MDP less negative than -65 mV). Thus, the sf_{Na} and sf_{CaL} are roughly determined by fitting the foot of AP and the timing of the rapid rising phase of AP. The plateau time course of AP is determined by sf_{CaL} and the factor of Ca^{2+} -mediated inactivation of I_{CaL} (the parameter KL , [4]). Since the kinetics of outward currents, I_{Kur} , I_{Kto} (*endo-type*), and I_{Ks} are quite different from that of I_{Kr} , the plateau configuration is determined bit by bit by adjusting these currents. We failed to observe the phase 1 rapid and transient repolarization in the hiPSC-CMs (Fig 2), which is the typical sign of the absence of epicardial-type I_{Kto} .

In hiPSC-CMs showing less negative MDP than ~ -65 mV, the contribution of I_{K1} , I_{Na} and I_{ha} should be negligibly small because I_{K1} is nearly completely blocked by the intracellular Mg^{2+} and polyamine, I_{Na} is inactivated, and I_{ha} is deactivated during SDD, even if any expressed.

Nevertheless, parameter optimization might be laborious and time-consuming for those who are not familiar with the electrophysiology of the cardiac myocyte. This difficulty might be largely eased by accumulating both AP configurations and the underlying current profile obtained in the parameter optimization into a database in the future. If this database becomes available, the computer may search for several candidate APs for the initial parameter set, which is used for automatic parameter optimization.

6. Funding and financial conflicts of interest

The authors declare that the research was conducted without any commercial or financial relationships that could be construed as a potential conflict of interest.

Improved identifiability of cardiac AP model parameters by physiological constraints

28

This work was supported by JSPS KAKENHI (Grant-in-Aid for Young Scientists) Grant Numbers JP19K17560 for HK, 16K18996 for YH, and 21K06781 for FT.

7. Author Contributions

HK, YH, DY, YW, AK, and TM performed the wet experiments and analyzed them. HK, SK, YH, YZ, FT, AA, and AN developed the simulation model and the parameter optimization method. HK, YH, AA and AN wrote the manuscript. All authors reviewed the manuscript. AA and TK organized the research team.

8. Acknowledgments

The authors would like to thank our laboratory colleagues for their valuable comments and discussions.

9. References

1. Noble D, Garny A, Noble PJ. How the Hodgkin-Huxley equations inspired the Cardiac Physiome Project: Hodgkin-Huxley equations and the cardiac Physiome Project. *J Physiology*. 2012;590: 2613–2628. doi:10.1113/jphysiol.2011.224238
2. Noble D, Rudy Y. Models of cardiac ventricular action potentials: iterative interaction between experiment and simulation. *Philosophical Transactions Royal Soc Lond Ser Math Phys Eng Sci*. 2001;359: 1127–1142. doi:10.1098/rsta.2001.0820
3. Winslow RL, Cortassa S, O'Rourke B, Hashambhoy YL, Rice JJ, Greenstein JL. Integrative modeling of the cardiac ventricular myocyte. *Wiley Interdiscip Rev Syst Biology Medicine*. 2011;3: 392–413. doi:10.1002/wsbm.122
4. Hinch R, Greenstein JL, Tanskanen AJ, Xu L, Winslow RL. A Simplified Local Control Model of Calcium-Induced Calcium Release in Cardiac Ventricular Myocytes. *Biophys J*. 2004;87: 3723–3736. doi:10.1529/biophysj.104.049973
5. Paci M, Hyttinen J, Aalto-Setälä K, Severi S. Computational models of ventricular- and atrial-like human induced pluripotent stem cell derived cardiomyocytes. *Ann Biomed Eng*. 2013;41: 2334–2348. doi:10.1007/s10439-013-0833-3

Improved identifiability of cardiac AP model parameters by physiological constraints

29

6. Paci M, Hyttinen J, Rodriguez B, Severi S. Human induced pluripotent stem cell-derived versus adult cardiomyocytes: an in silico electrophysiological study on effects of ionic current block. *Brit J Pharmacol.* 2015;172: 5147–5160. doi:10.1111/bph.13282
7. Lei CL, Wang K, Clerx M, Johnstone RH, Hortigon-Vinagre MP, Zamora V, et al. Tailoring Mathematical Models to Stem-Cell Derived Cardiomyocyte Lines Can Improve Predictions of Drug-Induced Changes to Their Electrophysiology. *Front Physiol.* 2017;8: 986. doi:10.3389/fphys.2017.00986
8. Grandi E, Pasqualini FS, Bers DM. A novel computational model of the human ventricular action potential and Ca transient. *Journal of molecular and cellular cardiology.* 2010;48: 112–121. doi:10.1016/j.yjmcc.2009.09.019
9. O'Hara T, Virág L, Varró A, Rudy Y. Simulation of the Undiseased Human Cardiac Ventricular Action Potential: Model Formulation and Experimental Validation. McCulloch AD, editor. *Plos Comput Biol.* 2011;7: e1002061-29. doi:10.1371/journal.pcbi.1002061
10. Asakura K, Cha CY, Yamaoka H, Horikawa Y, Memida H, Powell T, et al. EAD and DAD mechanisms analyzed by developing a new human ventricular cell model. *Prog Biophysics Mol Biology.* 2014;116: 11–24. doi:10.1016/j.pbiomolbio.2014.08.008
11. Himeno Y, Asakura K, Cha CY, Memida H, Powell T, Amano A, et al. A Human Ventricular Myocyte Model with a Refined Representation of Excitation-Contraction Coupling. *Biophys J.* 2015;109: 415–427. doi:10.1016/j.bpj.2015.06.017
12. Dokos S, Lovell NH. Parameter estimation in cardiac ionic models. *Prog Biophysics Mol Biology.* 2004;85: 407–431. doi:10.1016/j.pbiomolbio.2004.02.002
13. Dutta S, Chang KC, Beattie KA, Sheng J, Tran PN, Wu WW, et al. Optimization of an In silico Cardiac Cell Model for Proarrhythmia Risk Assessment. *Front Physiol.* 2017;8: 616. doi:10.3389/fphys.2017.00616
14. Whittaker DG, Clerx M, Lei CL, Christini DJ, Mirams GR. Calibration of ionic and cellular cardiac electrophysiology models. *Wiley Interdiscip Rev Syst Biology Medicine.* 2020;12: e1482. doi:10.1002/wsbm.1482
15. Cairns DI, Fenton FH, Cherry EM. Efficient parameterization of cardiac action potential models using a genetic algorithm. *Chaos Interdiscip J Nonlinear Sci.* 2017;27: 093922. doi:10.1063/1.5000354
16. Gábor A, Banga JR. Robust and efficient parameter estimation in dynamic models of biological systems. *Bmc Syst Biol.* 2015;9: 74. doi:10.1186/s12918-015-0219-2
17. Degasperi A, Fey D, Kholodenko BN. Performance of objective functions and optimisation procedures for parameter estimation in system biology models. *Npj Syst Biology Appl.* 2017;3: 20. doi:10.1038/s41540-017-0023-2
18. Penas DR, González P, Egea JA, Doallo R, Banga JR. Parameter estimation in large-scale systems biology models: a parallel and self-adaptive cooperative strategy. *Bmc Bioinformatics.* 2017;18: 52. doi:10.1186/s12859-016-1452-4
19. Villaverde AF, Fröhlich F, Weindl D, Hasenauer J, Banga JR. Benchmarking optimization methods for parameter estimation in large kinetic models. *Bioinformatics.* 2019;35: 830–838. doi:10.1093/bioinformatics/bty736

Improved identifiability of cardiac AP model parameters by physiological constraints

30

20. Sher A, Niederer SA, Mirams GR, Kirpichnikova A, Allen R, Pathmanathan P, et al. A Quantitative Systems Pharmacology Perspective on the Importance of Parameter Identifiability. *B Math Biol.* 2022;84: 39. doi:10.1007/s11538-021-00982-5
21. Coope ID, Price CJ. A direct search conjugate directions algorithm for unconstrained minimization. *Anziam J.* 2000;42: 478–498. doi:10.21914/anziamj.v42i0.609
22. Hough PD, Kolda TG, Torczon VJ. Asynchronous Parallel Pattern Search for Nonlinear Optimization. *Siam J Sci Comput.* 2001;23: 134–156. doi:10.1137/s1064827599365823
23. Groenendaal W, Ortega FA, Kherlopian AR, Zygmunt AC, Krogh-Madsen T, Christini DJ. Cell-Specific Cardiac Electrophysiology Models. *Plos Comput Biol.* 2015;11: e1004242. doi:10.1371/journal.pcbi.1004242
24. Sarkar AX, Sobie EA. Regression Analysis for Constraining Free Parameters in Electrophysiological Models of Cardiac Cells. *Plos Comput Biol.* 2010;6: e1000914. doi:10.1371/journal.pcbi.1000914
25. Zaniboni M, Riva I, Cacciani F, Groppi M. How different two almost identical action potentials can be: A model study on cardiac repolarization. *Math Biosci.* 2010;228: 56–70. doi:10.1016/j.mbs.2010.08.007
26. Krogh-Madsen T, Sobie EA, Christini DJ. Improving cardiomyocyte model fidelity and utility via dynamic electrophysiology protocols and optimization algorithms. *J Physiology.* 2016;594: 2525–2536. doi:10.1113/jp270618
27. Hooke R, Jeeves TA. ``Direct Search`` Solution of Numerical and Statistical Problems. *J Acm Jacm.* 1961;8: 212–229. doi:10.1145/321062.321069
28. Torczon V. On the Convergence of Pattern Search Algorithms. *Siam J Optimiz.* 1997;7: 1–25. doi:10.1137/s1052623493250780
29. Ma J, Guo L, Fiene SJ, Anson BD, Thomson JA, Kamp TJ, et al. High purity human-induced pluripotent stem cell-derived cardiomyocytes: electrophysiological properties of action potentials and ionic currents. 2011.
30. Hagiwara N, IRISAWA H, Kasanuki H, Hosoda S. Background current in sino-atrial node cells of the rabbit heart. *The Journal of physiology.* 1992;448: 53–72. doi:10.1113/jphysiol.1992.sp019029
31. Kiyosue T, Spindler AJ, Noble SJ, NOBLE D. Background inward current in ventricular and atrial cells of the guinea-pig. *Proceedings Biological sciences.* 1993;252: 65–74. doi:10.1098/rspb.1993.0047
32. Cheng H, Li J, James AF, Inada S, Choisy SCM, Orchard CH, et al. Characterization and influence of cardiac background sodium current in the atrioventricular node. *J Mol Cell Cardiol.* 2016;97: 114–24. doi:10.1016/j.yjmcc.2016.04.014
33. Tusscher KHWJ ten, Noble D, Noble PJ, Panfilov AV. A model for human ventricular tissue. *Am J Physiol-heart C.* 2004;286: H1573–H1589. doi:10.1152/ajpheart.00794.2003
34. Ashford JR, Colquhoun D. Lectures on Biostatistics: An Introduction to Statistics with Applications in Biology and Medicine. *J Royal Statistical Soc Ser Gen.* 1972;135: 606–606. doi:10.2307/2344687
35. Syed Z, Vigmond E, Nattel S, Leon LJ. Atrial cell action potential parameter fitting using genetic algorithms. *Medical Biological Eng Comput.* 2005;43: 561–571. doi:10.1007/bf02351029

Improved identifiability of cardiac AP model parameters by physiological constraints

31

36. Guo T, Abed AA, Lovell NH, Dokos S. Optimisation of a Generic Ionic Model of Cardiac Myocyte Electrical Activity. *Comput Math Method M.* 2013;2013: 706195. doi:10.1155/2013/706195
37. Beeler GW, Reuter H. Reconstruction of the action potential of ventricular myocardial fibres. *J Physiology.* 1977;268: 177–210. doi:10.1113/jphysiol.1977.sp011853
38. Faber GM, Rudy Y. Action Potential and Contractility Changes in [Na⁺]_i Overloaded Cardiac Myocytes: A Simulation Study. *Biophys J.* 2000;78: 2392–2404. doi:10.1016/s0006-3495(00)76783-x
39. Powell T, Twist VW. A rapid technique for the isolation and purification of adult cardiac muscle cells having respiratory control and a tolerance to calcium. *Biochem Bioph Res Co.* 1976;72: 327–333. doi:10.1016/0006-291x(76)90997-9
40. Sakmann B, Neher E. Patch Clamp Techniques for Studying Ionic Channels in Excitable Membranes. *Annu Rev Physiol.* 1984;46: 455–472. doi:10.1146/annurev.ph.46.030184.002323
41. Cha CY, Himeno Y, Shimayoshi T, Amano A, Noma A. A novel method to quantify contribution of channels and transporters to membrane potential dynamics. *Biophys J.* 2009;97: 3086–3094. doi:10.1016/j.bpj.2009.08.060
42. Winslow RL, Walker MA, Greenstein JL. Modeling calcium regulation of contraction, energetics, signaling, and transcription in the cardiac myocyte. *Wiley Interdiscip Rev Syst Biology Medicine.* 2016;8: 37–67. doi:10.1002/wsbm.1322
43. Hilgemann DW, Feng S, Nasuhoglu C. The Complex and Intriguing Lives of PIP2 with Ion Channels and Transporters. *Sci Stke.* 2001;2001: re19. doi:10.1126/stke.2001.111.re19
44. Suh B-C, Hille B. PIP2 Is a Necessary Cofactor for Ion Channel Function: How and Why? *Biophysics.* 2008;37: 175–195. doi:10.1146/annurev.biophys.37.032807.125859
45. Sasaki N, Mitsuiye T, Wang Z, Noma A. Increase of the delayed rectifier K⁺ and Na⁽⁺⁾-K⁺ pump currents by hypotonic solutions in guinea pig cardiac myocytes. *Circ Res.* 2018;75: 887–895. doi:10.1161/01.res.75.5.887
46. Hammami S, Willumsen NJ, Olsen HL, Morera FJ, Latorre R, Klaerke DA. Cell volume and membrane stretch independently control K⁺ channel activity: Cell volume, membrane stretch and K⁺ channel activity. *J Physiology.* 2009;587: 2225–2231. doi:10.1113/jphysiol.2008.163550
47. Peyronnet R, Nerbonne JM, Kohl P. Cardiac Mechano-Gated Ion Channels and Arrhythmias. *Circ Res.* 2016;118: 311–329. doi:10.1161/circresaha.115.305043
48. Gao J, Yun T, Xie X-L, Zhao J, Liu C, Sheng Y, et al. Losartan inhibits hyposmotic-induced increase of I_{Ks} current and shortening of action potential duration in guinea pig atrial myocytes. *Anatol J Cardiol.* 2020;23: 35–40. doi:10.14744/anatoljcardiol.2019.75332
49. Cannell MB, Kong CHT. Local control in cardiac E–C coupling. *J Mol Cell Cardiol.* 2012;52: 298–303. doi:10.1016/j.yjmcc.2011.04.014
50. Bers DM. Calcium Cycling and Signaling in Cardiac Myocytes. *Annu Rev Physiol.* 2008;70: 23–49. doi:10.1146/annurev.physiol.70.113006.100455

Improved identifiability of cardiac AP model parameters by physiological constraints

32

51. Greenstein JL, Hinch R, Winslow RL. Mechanisms of Excitation-Contraction Coupling in an Integrative Model of the Cardiac Ventricular Myocyte. *Biophys J*. 2006;90: 77–91. doi:10.1529/biophysj.105.065169
52. Negroni JA, Lascano EC. Simulation of steady state and transient cardiac muscle response experiments with a Huxley-based contraction model. *Journal of molecular and cellular cardiology*. 2008;45: 300–312. doi:10.1016/j.yjmcc.2008.04.012
53. Timmermann V, Edwards AG, Wall ST, Sundnes J, McCulloch AD. Arrhythmogenic Current Generation by Myofilament-Triggered Ca²⁺ Release and Sarcomere Heterogeneity. *Biophys J*. 2019;117: 2471–2485. doi:10.1016/j.bpj.2019.11.009
54. Niederer SA, Campbell KS, Campbell SG. A short history of the development of mathematical models of cardiac mechanics. *J Mol Cell Cardiol*. 2019;127: 11–19. doi:10.1016/j.yjmcc.2018.11.015
55. Hagiwara N, Irisawa H, Kameyama M. Contribution of two types of calcium currents to the pacemaker potentials of rabbit sino-atrial node cells. *J Physiology*. 1988;395: 233–253. doi:10.1113/jphysiol.1988.sp016916
56. Zhou Z, Lipsius SL. T-Type Calcium Current in Latent Pacemaker Cells Isolated from Cat Right Atrium. *J Mol Cell Cardiol*. 1994;26: 1211–1219. doi:10.1006/jmcc.1994.1139
57. Guo J, Ono K, Noma A. A sustained inward current activated at the diastolic potential range in rabbit sino-atrial node cells. *J Physiology*. 1995;483: 1–13. doi:10.1113/jphysiol.1995.sp020563
58. Toyoda F, Mesirca P, Dubel S, Ding W-G, Striessnig J, Mangoni ME, et al. CaV1.3 L-type Ca²⁺ channel contributes to the heartbeat by generating a dihydropyridine-sensitive persistent Na⁺ current. *Sci Rep-uk*. 2017;7: 7869. doi:10.1038/s41598-017-08191-8
59. Toyoda F, Wei-Guang D, Matsuura H. Heterogeneous functional expression of the sustained inward Na⁺ current in guinea pig sinoatrial node cells. *Pflügers Archiv - European J Physiology*. 2018;470: 481–490. doi:10.1007/s00424-017-2091-y
60. Guinamard R, Bouvagnet P, Hof T, Liu H, Simard C, Sallé L. TRPM4 in cardiac electrical activity. *Cardiovasc Res*. 2015;108: 21–30. doi:10.1093/cvr/cvv213
61. Doss MX, Diego JMD, Goodrow RJ, Wu Y, Cordeiro JM, Nesterenko VV, et al. Maximum diastolic potential of human induced pluripotent stem cell-derived cardiomyocytes depends critically on I(Kr). Barbuti A, editor. *Plos One*. 2012;7: e40288. doi:10.1371/journal.pone.0040288
62. Ishihara K, Yan D, Yamamoto S, Ehara T. Inward rectifier K⁺ current under physiological cytoplasmic conditions in guinea-pig cardiac ventricular cells. *J Physiology*. 2002;540: 831–841. doi:10.1113/jphysiol.2001.013470